Dynamic model for convective heating of a wet brick during energy characterisation of domestic electric ovens

Dynamic Model for Convective Heating of a Wet Brick during Energy Characterisation of Domestic Electric Ovens

M. Lucchi[a], N. Suzzi[b], M. Lorenzini[a,*]

[a] *Alma Mater Studiorum Universitá di Bologna - DIN - Via Fontanelle 40, Forlí- I-47121 - ITALY*
[b] *DPIA-Dipartimento Politecnico di Ingegneria e Architettura, Universitá di Udine, Via delle Scienze, Udine, Italy*

Abstract

Electric ovens usually represent a low-efficiency category among household appliances, influencing the overall environmental impact of buildings. The energy class of such devices is determined through a test procedure defined by the EN 60350 European standard, where a wet clay brick is heated under set conditions and accurate control of the air temperature during the test is required, which marks the importance of efficient control strategies. In this work a control-oriented dynamic model was devised to predict the transient thermal behaviour of the oven during energy consumption tests carried out in forced-convective mode, including the heat and mass transfer occurring between the wet brick and the cavity air. Model parameters were determined through an optimisation procedure based on experimental data. Comparisons with other sets of experimental data also allowed to validate the predictive capability of the model. The model predicts well the temperature of the cavity air, the Pt500 probe used as a temperature feedback and the core temperature of the brick with deviations lower than 10% after the heating phase of the cavity. The brick heating time and water loss are also captured by the model, with deviations lower than 6% for the former and 9% for the latter.

Keywords: energy efficiency, heat transfer in appliances, transient thermal analysis, forced convection, thermal control, evaporation.

1. Introduction

Among the household appliances, which are responsible of almost 25% of the overall environmental impact of buildings, [1], electric ovens rank among the worst in terms of energy efficiency, with values between 10% and 12%. This has spurred investigation of more efficient technologies, [2, 3]. The efficiency of the appliance is rated through its energy class, which ranges from A+++ (best) to D and is certified in the EU through a test regulated by the EN 60350 standard. This mandates measurement of the electric power consumption in the heating of a standard wet brick under different functions and, among others, strictly requires a proper control of the air temperature in the cavity, [4]. For manufacturers, performing the tests for different oven models and the trial-and-error approaches employed to design of oven control strategies demand a vast amount of time and resources, thus making the use

* Corresponding author *Email address:* marco.lorenzini@unibo.it (M. Lorenzini)

of simulation tools highly desirable. The aim of this work is to obtain a reliable dynamic model to predict the transient thermal behaviour of the oven during energy consumption tests, focusing on the main temperatures of the oven cavity and the brick, and taking into account the water loss as well.

The transient thermal behaviour of domestic ovens has been the focus of many investigations in literature, both experimental and numerical. Among the former, the work presented by Cernela et al., [5], proposed test procedures for the evaluation of the heating performance during oven-baking and pan-frying, relying on the measurements of the air temperature, the equivalent radiative temperature and the convective heat transfer coefficients in the cavity.

With regards to numerical approaches, several works of different levels of complexity can be found. The work by Abraham and Sparrow, [6], uses a simple energy balance to estimate the temporal evolution of temperature for a thermal load heated inside an electric oven, which operates in natural-convective mode. Yet, no information about the air temperature can be obtained through the model; moreover, the radiative heat transfer was described by linearised terms.

To the opposite end of the complexity scale lie the works by Mistry et al., which investigated in detail through CFD models the transient natural convection during the broiling and baking cycles in electric ovens, [7], and the heat transfer and fluid flow within a household gas oven, [8].

When dealing with control design, a compromise between model accuracy and simplicity must be struck. Thus, the deep insight into thermal phenomena that CFD or FEM models usually ensure, as shown in [9], must be set aside in favour of lower-order models. When energy analysis at system level are carried out, models based on the lumped-parameter approach are often used, [10, 11]. In [12], a lumped-parameter model of a professional oven with no internal load was developed, considering the radiative heat exchanges through non-linearised terms. After a tuning procedure of the model parameters, numerical results showed good agreement with the experimental data, even if the validation proposed in the paper was carried out at a single temperature set-point. The work by Laboreo et al., [13] represents another example of the application of the lumped-parameter approach to model the transient behaviour of ovens. On the basis of one of their previous works, [14], they used the thermoelectric analogy to carry out a transient energy analysis of the oven, also introducing the dynamics of the wet brick employed in the energy consumption test, considering both the forced convective and radiative cooking processes. However, no information can be extracted from the model on the actual air temperature surrounding the thermal load and on the temperature sensed by the probe used to keep the desired set-point, thus making its use for control design difficult. Moreover, no temperature trends were reported for the brick.

In this work, a control-oriented, low-order model was developed in MATLAB/Simulink® to analyse the transient thermal behaviour of the oven during a standard energy consumption test. With respect to the work presented by the authors in [15], the heat and mass transfer involving the wet brick was

introduced in the model, thus increasing its complexity and capabilities. In particular, the mass of the absorbed water was included in the brick's thermal capacity and the water evaporation rate was evaluated considering the vapour partial pressures at the brick surface and in the cavity air. A lumped-parameter approach was used for both the brick and the cavity and, differently from [13], a certain level of discretization was introduced in order for the model to be able to predict the main temperatures necessary to its thermal control. In particular, among others, the brick's core temperature (on which the duration of the test is based), the temperature of the air in the cavity and the temperature sensed by the probe used by the oven control board to maintain the desired set-point can be predicted by the model. The predictive capability of the model in terms of temperatures, water loss and heating time of the brick confer a clear innovative contribution to the work. Similarly to what presented in [15], a "grey-box" modeling approach was chosen, since it allows the description of the complex physical phenomena occurring in thermal systems, e.g. in refrigeration [16]. The parameters appearing in the model equations and deriving from energy and mass balances, were determined through an optimisation procedure based on experimental data obtained during energy consumption tests carried out with the oven in forced-convective heating mode. The model was then validated at different temperature set-points.

2. The EN 60350 energy consumption test

The energy class of an electric domestic oven is usually determined through the test described in the EN 60350 European Standard, [4]. During the test, a clay brick acting as thermal load with dimensions 230 mm x 114 mm x 64 mm and 920 ± 75 g weight is soaked in cold water for at least 8 hours, to obtain an increase in weight of 1050 ± 50 g and a core temperature of $5 \pm 2°C$. Subsequently, the brick is heated in the oven until its core temperature reaches an increase of 55 K, weighed again thereafter to determine the loss in water, and the electric energy consumption of the oven during the process is recorded. As summarised in Tab. 1, the standard requires the test to be carried out both in forced- and natural-convective heating modes and under different temperature set-points ΔT_{set}, considered as temperature increments above the ambient temperature T_{AMB}, which must be kept at 23 ± 2°C. However, taking into account the tolerances allowed by the standard, the temperature set points T_{set} usually investigated by the manufacturers are $160 - 180 - 200$°C and $160 - 200 - 240$°C for forced- and natural-convective heating respectively. The energy class is then determined on the basis of the electrical consumption measured during the tests and of the cavity volume through a correlation given by the standard. Because of its increased thermal losses due to the higher convective heat transfer in the cavity, which contribute to decrease the energy efficiency, the forced convective heating mode is usually of major interest for manufacturers and will be the focus of this work.

Table 1: Set-points for the energy consumption test, as prescribe by the EN 60350 European Standard.

	$\Delta T_{set} \pm 10\,(\mathrm{K})$	Usual set points $T_{set}\,(^{\circ}\mathrm{C})$
Forced Convection	135-155-175	160-180-200
Natural Convection	140-180-220	160-200-240

3. Experimental setup

A commercial household oven ("Electrolux - EOB6850BOX") with an inner cavity of 72 dm^3 was used in the experiments, setting it into a piece of furniture to reproduce the same conditions of a kitchen. The appliance has three heating elements, namely a 1900 W ring heater (RH), a 2300 W top heater (TH) and a 1000 W bottom heater (BH): in the forced-convective cooking function investigated, only the ring heater, together with the fan, is activated. Figure 1 highlights the relative positions among the main components of the oven cavity, such as walls, glass door, heaters and the Pt500 probe. The latter is the only temperature feedback for the oven control board during operation and therefore instrumental to keep the cavity temperature at the set-point value.

In addidion to the Pt500 sensor, temperature measurements were carried out through K-type thermo-

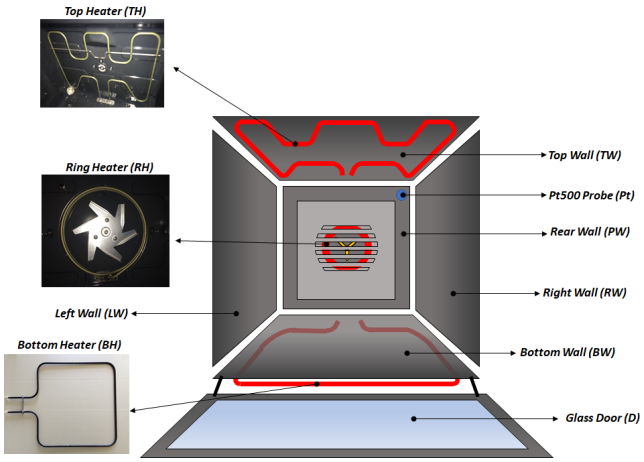

Figure 1: Sketch of the oven cavity highlighting the relative position of the main elements.

couples: the detailed description of their location on the cavity walls and heaters can be found in [15]. During the energy consumption test, the actual oven centre (OC) temperature cannot be measured because of the presence of the brick. Therefore, four thermocouples were placed perpendicular to the grid onto which the brick is laid during the test, about 2 cm from its side. The average value of the four recordings from the thermocouples was then considered as representative of the oven centre.

For a complete thermal characterisation of the brick through a lumped-parameter model, as detailed in section 4.2, knowledge of both its core and surface temperature was needed. Two thermocouples were therefore placed at a depth of about 32 mm, as prescribed by the standard, [4], and one thermocouple was embedded at surface level into each of the brick's faces, as shown in Fig. 2.

Apart from the Kapton®tape used to fix them, no particular radiation shielding was used for thermocouples. Indeed, considering thermocouples placed on the surfaces of walls, heating elements and the brick, assuming an ideal contact between the sensor head and the surfaces to monitor, the probe would be at thermal equilibrium with the body considered. Also, the radiative contribution has been neglected for the air temperature measurements, because of the consistency obtained in absence of thermal load between the value sensed by the thermocouple at the oven centre and the temperature of the Pt500 probe. For each element of the oven, the arithmetic mean of the measured temperatures was used as representative value.

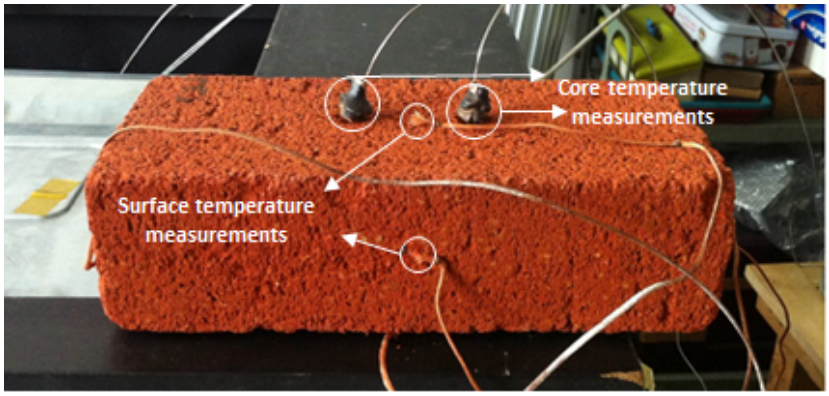

Figure 2: Details of thermocouples location on the brick.

As for the electric power measurement, four LogiLight EM0002 power meters were used to record the overall electric power absorbed and the electric power consumption of each heating element, which were then used as model inputs.

The sampling time of the whole measurement chain was 2 s, whilst detailed information about the acquisition system can be found in [17]. The overall uncertainty on measurements can be calculated without any sensitivity coefficients involved, as done for other cases, [18], and in Tab. 2 the values obtained for temperature and power after calibration are reported.

The tests were carried out in an air-conditioned room at a controlled temperature $T_{AMB} = 23 \pm 1°C$, and three temperature set points, T_{set}, were investigated, namely $160 - 180 - 200\,°C$, according to the standard for the forced-convective heating functions. Similarly to what presented in [15], one set of experimental data ($T_{set} = 180°C$) was used to identify the parameters of the grey-box model through an optimisation algorithm as discussed in 4.3. The remaining two sets were then used for

Table 2: Overall uncertainty of measurements.

Temperature	$\pm 1.0\,^{\circ}\mathrm{C}$ up to $240\,^{\circ}\mathrm{C}$
	Maximum of $\pm 4.5\,^{\circ}\mathrm{C}$ in the range $1 - 500\,^{\circ}\mathrm{C}$
Electric Power	$\pm 0.5\%$

model validation. In each case, the electric power absorbed by the ring heater was used as input to the models, the room temperature is treated as a perturbation, whilst the outputs of the model are the temperatures of the cavity, the brick and the heaters.

4. Model

In line with what was presented in [15], the lumped-parameter approach based on the thermoelectric analogy was adopted to construct a control-oriented model with a sufficient level of discretization to predict the main temperatures of the cavity (e.g. oven centre and Pt500 temperature) and the brick. The oven cavity was represented through ten nodes, namely the cavity air (OC), the Pt500 sensor (Pt), the five cavity walls and the glass door (D), the ring heater (RH) and, although inactive in the heating function considered, the top heater (TH), in order to allow the possible study of ventilated cooking functions with grilling, which are of interest for manufacturers.

The brick model is described by two thermal nodes, related to its core (BrC) and its outer part (BrS), and by a dynamic variable representing the evaporated mass of water ($m_{w\,ev}$). The overall model had order 13 and was implemented in MATLAB/Simulink®.

4.1. Oven model

The energy balance for a generic node i of the thermoelectric grid of the oven can be expressed through Eq. (1), where the convective-conductive heat transfer $\dot{Q}_{i\ j}$, the radiation $\dot{Q}^{rad}_{i\ j}$ exchanged between two generic nodes i and j and the absorbed electric power $\dot{W}_{el\,i}$ all contribute to the variation of the node internal energy, which depends on its thermal capacity C_i. Clearly, the term $\dot{W}_{el\,i}$ takes non-zero values only for the nodes associated with the heaters.

$$C_i \frac{dT_i}{d\tau} = \sum_{j=1}^{n} (\dot{Q}_{i\ j} + \dot{Q}^{rad}_{i\ j}) + \dot{W}_{el\,i} \tag{1}$$

The heat transfer $\dot{Q}_{i\ j}$ due to convection and conduction between two generic nodes i and j is calculated through Eq. (2) as a function of the thermal conductance $G_{i\ j}$ between nodes i and j and

of the corresponding temperatures T_i and T_j.

$$\dot{Q}_{i\ j} = G_{i\ j} \cdot (T_j - T_i) \tag{2}$$

The generic radiative heat exchange $\dot{Q}^{rad}_{i\ j}$ between two nodes of the thermoelectric circuit is instead calculated through Eq. (3), where the node temperatures T_i and T_j are expressed in degrees Kelvin, σ is the Stefan-Boltzman constant and $G^{rad}_{i\ j}$ is the radiative thermal conductance between nodes i and j calculated by means of Eq. (4), where ε_i and ε_j are the surface emissivities of the generic nodes i and j, A_i and A_j are the emission areas and F_{ij} is the view factor between surfaces i and j. Both types of conductances obey a reciprocity law, so that $G_{i\ j} = G_{j\ i}$ and $G^{rad}_{i\ j} = G^{rad}_{j\ i}$.

$$\dot{Q}^{rad}_{i\ j} = G^{rad}_{i\ j} \cdot \sigma \cdot (T_j^4 - T_i^4) \tag{3}$$

$$G^{rad}_{i\ j} = \frac{1}{\frac{1-\varepsilon_i}{\varepsilon_i A_i} + \frac{1}{F_{ij} A_i} + \frac{1-\varepsilon_j}{\varepsilon_j A_j}} \tag{4}$$

The significant radiative exchanges during the energy consumption test in forced convection heating mode are those related to cavity elements (walls, glass door and top heater) and the brick surface (BrS), which has a markedly lower temperature. To evaluate the radiative thermal conductances $G^{rad}_{i\ j}$, on the basis of information given by the manufacturer of the oven analysed, the emissivities assumed are 0.11 for the walls, 0.13 for the inner side of the door, 0.9 for the heaters and 0.6 for the brick. The view factors F_{ij} were estimated through the MATLAB® script proposed by Lauzier [19], assuming all the involved surfaces as planar.

In Tab. 3, the thermal connections for the nodes of the thermoelectric circuit of the oven are reported. It can be noticed how the heat source term $\dot{W}_{el\,i}$ appears only in the energy balance of

Table 3: Thermal connections for the nodes of the thermoelectric grid of the oven

Nodes	$\dot{Q}_{i\ j}$	$\dot{Q}^{rad}_{j\ i}$	$\dot{W}_{el\,i}$
Cavity Air (OC)	Cavity walls, glass door, ring and top heaters, brick surface	-	-
Pt500 (Pt)	Cavity air and rear wall	-	-
Ring Heater (RH)	Cavity air, walls, glass door, top heater	-	$\dot{W}_{el\,RH}$
Top Heater (TH)	Cavity air, ring heater	Brick surface	-
Cavity walls	Cavity air, ring heater, ambient	Brick surface	-
Glass Door (D)	Cavity air, ring heater, ambient	Brick surface	-

the ring heater, while the top heater is a mere capacitive load. As for the dynamics of the Pt500 sensor, a term directly connecting the sensor to the wall on the rear of the cavity is considered in addition to that for the oven centre. Indeed, the temperature sensor is located close to the rear wall PW (see Fig. 1), which is the hottest among cavity walls when only the ring heater is activated, as shown in Fig. 3, where the main temperatures within the cavity during an energy consumption test at $T_{set} = 180°C$ are reported. A significant difference between the air temperature and the value sensed

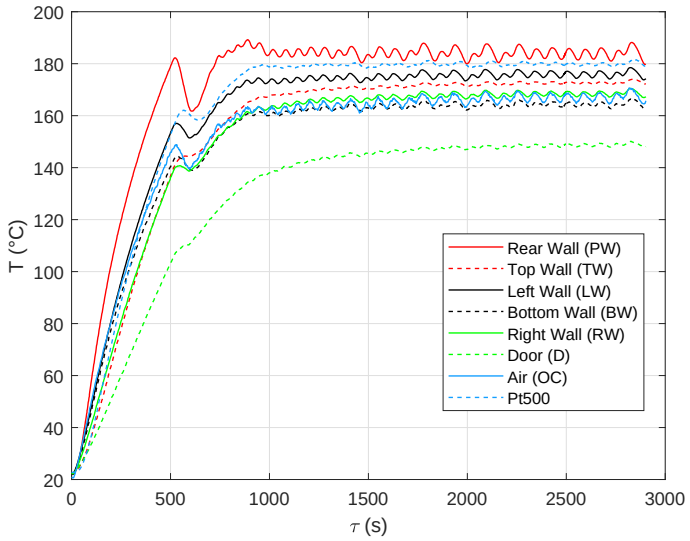

Figure 3: Main temperatures within the cavity during an energy consumption test carried out with the oven in forced convective heating mode (fan and ring heater activated). $T_{set} = 180°C$ and $T_{AMB} = 23°C$.

by the Pt500 sensor is also highlighted. In particular, once the oven reaches steady-state conditions, the temperature of the Pt500 coincides with the temperature set-point ($T_{set} = 180°C$ in Fig. 3), whilst the air temperature is about 15°C lower, because of the heat exchange with the colder, wet brick. A temperature difference between the right and left walls of about 10°C is also highlighted; this is due to the swirl imposed by the fan to the cavity air and to the asymmetric shape of metal sheet covering the fan which involve different heat transfer conditions at the two surfaces. This aspect fully justifies the use of two different thermal nodes for the left and right walls. Moreover, the temperature of the main elements of the cavity shows a relative minimum after the first 600 s, which is more pronounced the closer the element is to ring heater. Indeed, the control strategy adopted by the manufacturer is essentially the composition of two subsequent stages, which differ in the duty cycle adopted to operate the resistance. In the first stage, the heater is in operation for a longer time to reduce the duration of the oven warm up, whilst in the second one a lower mean heating power is delivered to keep the desired set-point. The minimum thus appears after the switch between the two control strategies.

4.2. Brick model

During the energy consumption test, the brick undergoes a process consisting of a combination of four main mechanisms:

- transient thermal diffusion;
- water diffusion through a porous medium;
- water evaporation at the outer surface due to the hot air flowing around the brick;
- water drip.

In order to capture the main dynamics of the process while keeping a certain degree of simplicity, the water drip effect was neglected and the lumped parameter approach was still used to model the heat diffusion and the water loss within the brick. In particular, as shown in Fig. 4, the brick was modelled through two different nodes. One node is associated with the brick's outer part (BrS), which is thermally connected with the walls and the top heater through radiation and with the air through convection: this is where actual evaporation occurs. The second node represents the bricks core (BrC): water diffuses from here to the brick's surface, which heats the core in turn.

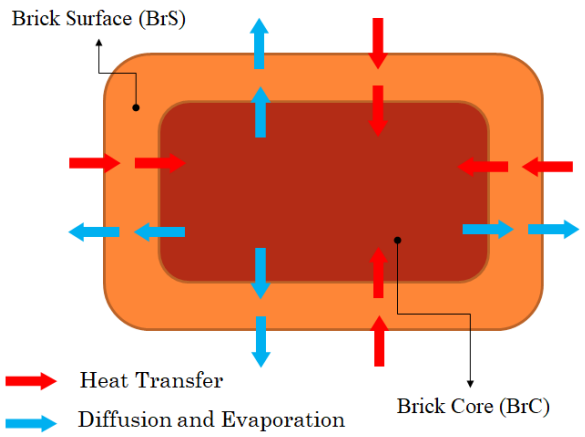

Figure 4: Scheme of the brick model.

One of the main assumptions made was to consider the mass flow rate of water spreading through the brick equal to the water evaporation rate. Thus, since water is supposed to diffuse from core to the surface, where evaporation occurs, during the process the inner node of the brick undergoes a decrease in its thermal capacity depending on the evaporated mass of water $m_{w\,ev}$, whilst the capacity of BrS

is assumed to remain constant.

Equation (5) is the energy balance for BrS, with its thermal capacity expressed as a function of the total mass of the dry brick m_{dry}, the specific heat capacity of the dry brick c_{dry} ($800\,\mathrm{J}\cdot\mathrm{kg}^{-1}\cdot\mathrm{K}^{-1}$, as per manufacturer's data), the total mass of water absorbed m_w, the specific heat capacity of water c_w and a parameter r which takes into account the mass distribution between the two parts of the brick. The parameter r can be defined as the ratio between the mass associated to the outer part of the brick, m_{BrS}, and its total mass, m_{Br}, as shown in Eq. 6.

$$\begin{aligned} r(m_{dry}c_{dry} + m_w c_w)\frac{dT_{BrS}}{d\tau} =& \dot{Q}_{OC\,BrS} + \dot{Q}_{BrC\,BrS} + \dot{Q}^{rad}_{TH\,BrS} + \dot{Q}^{rad}_{TW\,BrS} + \dot{Q}^{rad}_{BW\,BrS} + \dot{Q}^{rad}_{RW\,BrS} \\ &+ \dot{Q}^{rad}_{LW\,BrS} + \dot{Q}^{rad}_{PW\,BrS} + \dot{Q}^{rad}_{D\,BrS} - \dot{m}_w \Delta h_{lv} \end{aligned} \tag{5}$$

$$r = \frac{m_{BrS}}{m_{Br}} \tag{6}$$

As highlighted in Eq. (5), in addition to the thermal power which BrS exchanges with the elements of the cavity and the brick's core, to account for water evaporation at the surface the term $\dot{m}_w \Delta h_{lv}$ is introduced. In particular, Δh_{lv} is the enthalpy of vaporization at a mean brick's core temperature of 30°C (assumed as constant in the temperature range experienced by the brick during operation) and $\dot{m}_w$ is the mass flow rate of evaporating water. Since the diffusion and evaporation mass flow rates was assumed equal, $\dot{m}_w$ can be evaluated through Eq. (7), which is often used in the design of drying plants, [20].

$$\dot{m}_w = D A_{Br}(P_{BrS} - P_{v\,air}) \tag{7}$$

In Eq. (7), $\dot{m}_w$ is a function of D, mainly depending on the air flow around the brick, of the brick's outer surface A_{Br}, of the water saturation pressure P_{BrS} at the brick's surface temperature and of the partial pressure of water vapour in the air cavity $P_{v\,air}$. In this work, a constant partial vapour pressure $P_{v\,air}$ was considered for the air in the cavity, taking a value corresponding to a 50% relative humidity in ambient air at 23°C. In other words, the steam evacuation system of the oven is assumed to maintain a constant vapour mass and thus a constant absolute humidity within the cavity, if the mass of dry air remains fixed as well. The effects of a variable vapour partial pressure $P_{v\,air}$ on model accuracy will be investigated in the future. The calculation of the vapour saturation pressure $P_{BrS}\,(Pa)$ as a function of the brick's surface temperature was carried out at each time step through a fitting polynomial obtained from water property tables, as shown in Eq. (8), with T_{Br} in degrees

Celsius.

$$P_{BrS} = 0.001T_{BrS}^4 - 0.0313T_{BrS}^3 + 3.4453T_{BrS}^2 + 19.748T_{BrS} + 671.54 \tag{8}$$

Finally, Eq. (9) is the energy balance for the brick's core BrC, whose thermal capacity decreases in time depending on the amount of evaporated water $m_{w\,ev}$, which can be calculated by means of the mass balance of Eq. (10).

$$[(1-r)(m_{dry}c_{dry} + m_w c_w) - m_{w\,ev}c_w]\frac{dT_{BrC}}{d\tau} = \dot{Q}_{BrS\,BrC} \tag{9}$$

$$\frac{dm_{w\,ev}}{d\tau} = \dot{m}_w \tag{10}$$

Figure 5 reports a scheme of the whole model, showing the heat and mass transfer among the components. Thermal connections between the brick surface and the nodes of the oven were highlighted in red.

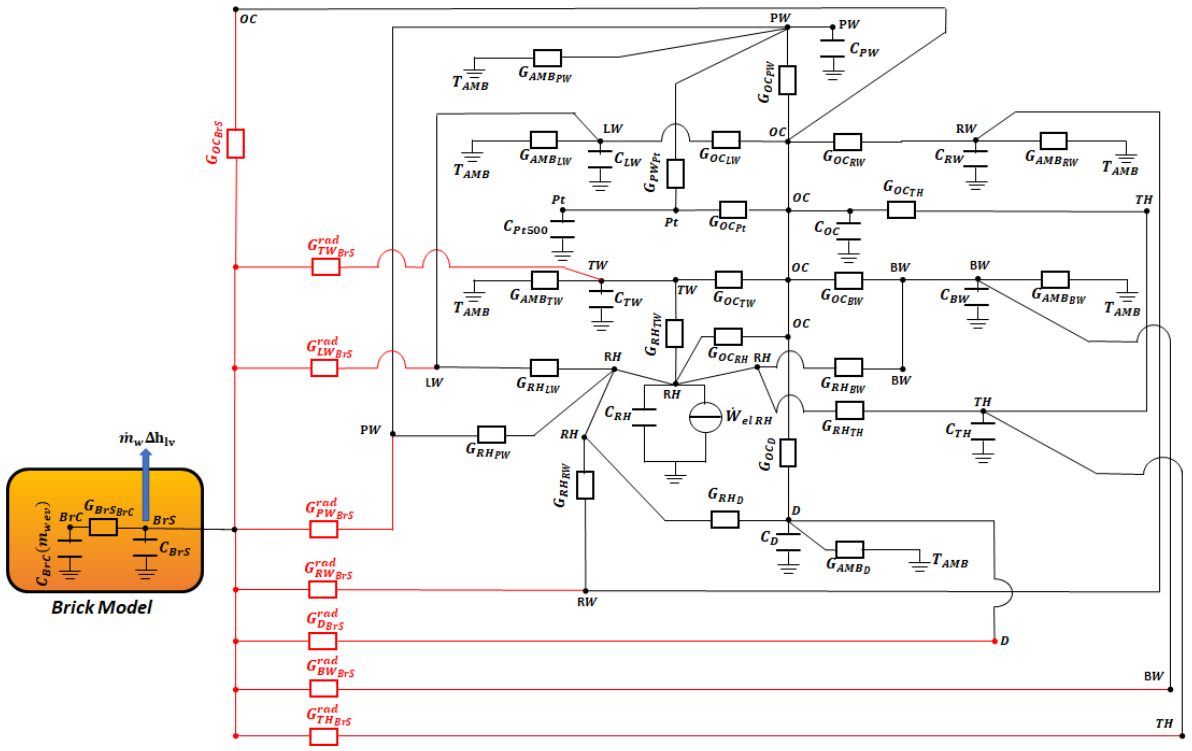

Figure 5: Schematic of the whole lumped parameter model.

4.3. Parameters identification

Model parameters were determined on the basis of experimental data acquired during an energy consumption test carried out at $T_{set} = 180°\mathrm{C}$. The masses of the dry brick, m_{dry}, and wet brick, m_{Br}, were measured at the beginning of the test; the calculation of the total amount of water absorbed m_w was then obtained straightforwardly as $m_w = m_{Br} - m_{dry}$. The evaporation coefficient D was estimated from the knowledge of the total mass of loss water $m_{w\,ev\,tot}$, which was calculated at the end of the test by subtracting the mass of the whole heated brick to the total mass of the brick m_{Br} measured at the beginning of the test. Integrating Eq. (7) over the duration of the test τ_f leads to Eq. (11), where P^{exp}_{BrS} is the instantaneous water saturation pressure at the experimental temperature of the brick's surface, T^{exp}_{BrS}, allowing an estimate for D.

$$D = \frac{m_{w\,ev\,tot}}{A_{Br} \int_0^{\tau_f} (P^{exp}_{BrS}(\tau) - P_{v\,air}) d\tau} \tag{11}$$

Except for the radiative thermal conductances G^{rad}_{ij} which were calculated as explained in section 4.1, all the capacities C_i, the linear thermal conductances G_{ij} and the mass distribution factor of the brick, r, were determined, with the same approach described in detail in [15]. In particular an optimisation procedure based on the Non-Linear-Least-Squares method was carried out in the Parameter Estimation framework available in MATLAB/Simulink®. Calling n the number of lumped parameters in the model, $T^{model}_i(k)$ and $T^{exp}_i(k)$ respectively the predicted and experimental temperature for the i-th parameter at the generic time-step k and N the total number of time-steps, the minimized cost function f is:

$$f = \sum_{i=1}^{n} \cdot \frac{\sum_{k=1}^{N} (T^{model}_i(k) - T^{exp}_i(k))^2}{N} \tag{12}$$

Also in the present work, a quite large range of variability was given to the parameters during the optimisation procedure, because the model mainly aimed at reliably predicting the cavity's and brick's temperatures in response to a particular electric power forcing function in input. Under these considerations, if the temperatures are predicted well, the model can be used to predict the overall electric energy consumption as well.

The solver used for the time-integration was a fixed-step Runge-Kutta method (Matlab ode4) and a time-step of 1 s was used. In the optimisation procedure, the simulation spanned the duration τ_f of the test, whereas in the model validation and to estimate the model-predicted brick heating time the duration of the simulation was manually tuned to simulate a temperature increment at the brick's core of at least $55\,K$.

5. Results

To evaluate the reliability of the model, the absolute value of the deviation Δ between numerical and experimental temperatures, the brick heating time and the total water loss have been used as indicators. In the following sections, results of the parameter identification and model validation will be presented.

5.1. Parameter identification

Figure 6 shows a comparison between the temperature predicted by the model for the air in the cavity and either the Pt500 probe (a) or the brick's temperatures (b) in the parameters identification procedure carried out at $T_{set} = 180°C$. A very good agreement is shown for both the air and the probe, with absolute deviations below 6 K and 3 K respectively. The temperature deviation of about 10 K between the temperature sensed by Pt500 and that of the air in steady-state conditions, already highlighted in Fig. 3, is also captured by the model.

Regarding the brick, a maximum deviation of about 6 K is obtained for T_{BrS} at the beginning of the

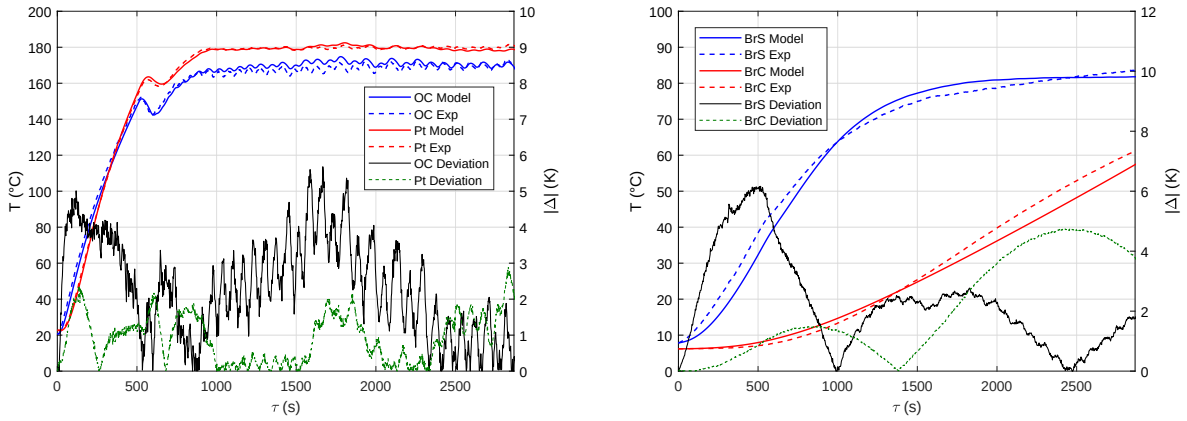

(a) (b)

Figure 6: Comparison between experimental and predicted temperatures of cavity air and Pt500 (a) and of brick's surface and core (b). Energy consumption test in forced-convective heating mode at $T_{set} = 180°C$ and $T_{AMB} = 23°C$.

simulation, whilst the core temperature T_{BrC} is captured by the model with a maximum deviation below 5 K at the end of the test. Since the curve related to the numerical results lays below the experimental one, this entails a slight overestimation of the time required to obtain a 55 K temperature increment at the brick's core.

The evaporated mass of water $m_{w\,ev}$ estimated through Eq.(10) is reported in Fig. 7 with a trend qualitatively similar to those obtained experimentally by Laboreo et al. in [13]. It can be noticed how evaporation is modest in the first 500 s of the simulation, where the temperature at the brick's surface

and thus the water saturation pressure is still low. Once T_{BrS} exceeds 35 °C , evaporation starts to increase, becoming almost linear in time after $\tau = 1500$ s.

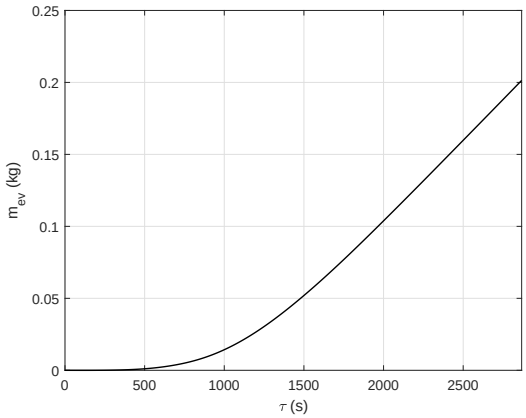

Figure 7: Predicted temporal trend of the water mass loss through evaporation during an energy consumption test in forced-convective heating mode at $T_{set} = 180$°C and $T_{AMB} = 23$°C.

Figure 8 shows the results obtained for two different nodes of the thermoelectric grid, namely the glass door (D) and the right wall (RW). It can be noticed how the temperature of the glass door is always lower than that of the right wall, because of the action of the door cooling system. Highest deviations of about 4 K are highlighted for both nodes in the first 1000 s, whilst in the steady-state regime the deviation reaches values lower than 3 K.

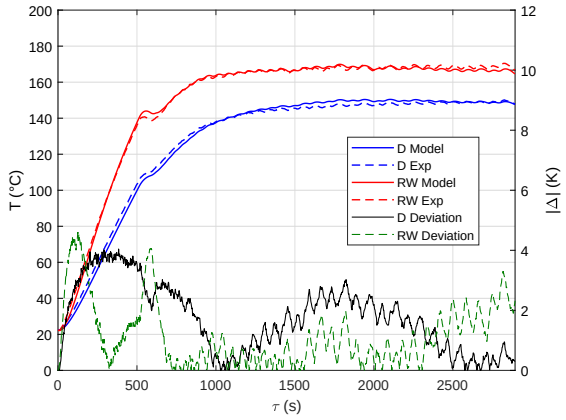

Figure 8: Comparison between experimental and predicted temperatures of the door and the right wall. Energy consumption test in forced-convective heating mode at $T_{set} = 180$°C and $T_{AMB} = 23$°C.

5.2. Model validation

Figure 9 shows the results obtained in validations tests for the air in the oven cavity and for the Pt500. For the test at $T_{set} = 160°C$ (see Fig. 9 (a)), maximum deviations lower than 8 K and 5 K are highlighted for the air and the probe respectively. From the curves of Fig. 9 (b), it can be noticed how the deviation between numerical and experimental data increases in the test at $T_{set} = 200°C$: a maximum value of about 15 K is highlighted for the air whilst the maximum deviation for the Pt500 is about 9 K. This behaviour may be due to an underestimation of the evaporative heat loss which leads to an overestimation of the brick's surface temperature when the set-point is increased. Possible improvements could be obtained introducing temperature-dependent values for the water evaporation coefficient D and the water vapour partial pressure $P_{v\,air}$ used in Eq. (7): further investigations will be carried out presently. Moreover, as it happens in the experiment, the estimated temperature for the Pt500 probe is still higher than the estimated air temperature: the model can therefore be useful to design effective controls for the air temperature.

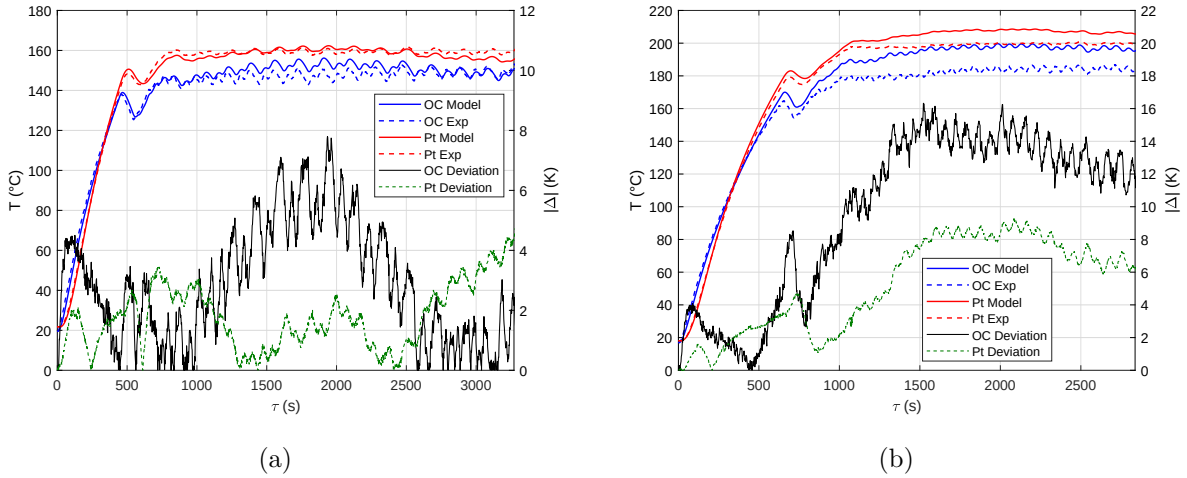

Figure 9: Predictive capabilities of the model: model-predicted and experimental temperature of the cavity air and Pt500 probe in energy consumption tests in forced-convective heating mode at $T_{set} = 160°C$ (a) and $T_{set} = 200°C$ (b). Ambient temperature kept at $T_{AMB} = 23°C$.

Figure 10 shows the results obtained for the brick temperatures. As expected, at $T_{set} = 160°C$ the temperature predicted by the model for the brick's surface is very close to the experimental trend (see Fig. 10 (a)), whilst in the test at $T_{set} = 200°C$ an overestimation up to 6.5 K is highlighted when the air in the cavity has already reached its steady-state regime. This justifies the behaviour discussed for the temperatures of the air and the Pt500. As for the brick's core temperature T_{BrC}, maximum deviations slightly above 4 K for the case at $T_{set} = 160°C$ and about 6.5 K for the test at $T_{set} = 200°C$ were highlighted. Also, in the validation test at lower temperature, the curve related to

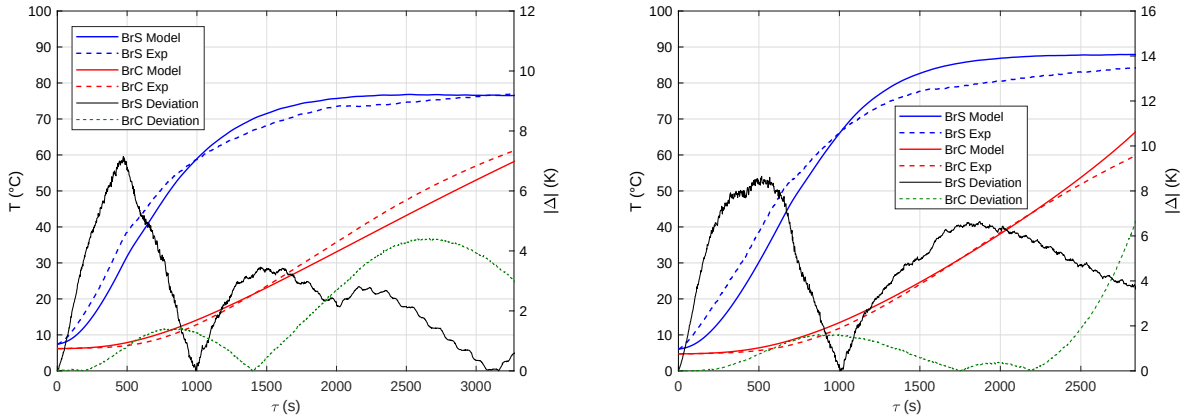

Figure 10: Predictive capability of the model: model-predicted and experimental temperature of the brick's surface in energy consumption tests in forced-convective heating mode at $T_{set} = 160°C$ (a) and $T_{set} = 200°C$ (b). Ambient temperature maintained at $T_{AMB} = 23°C$.

the numerical results lies below the experimental one at the end of the simulation, thus denoting an overestimation of the time required to heat the brick. An opposite behaviour is noticed for the test at higher temperature.

The results in terms of temperature prediction can be considered satisfactory for control-design purposes and taking into account the lumped-parameter nature of the model. Indeed, considering the air and brick's core temperatures, the percentage deviations obtained with respect to experimental data (lower than 10% after the heating phase of the cavity) is comparable with those obtained through CFD models [7].

In Tab. 4, the deviations between the experimental and numerical values of the brick heating time τ_f and total water loss $m_{w\,ev\,tot}$ are reported for all the tests. Percentage deviations lower than 6% are obtained for τ_f, which proves the model reliable in the prediction of the energy consumption test duration. As for the total amount of evaporated water, deviations lower than 9% were shown, which confirms the validity of the model in describing the evaporative process. In addition, an underestimation of $m_{w\,ev\,tot}$ is highlighted in the test at $T_{set} = 200°C$: this is consistent with the temperature overestimation shown for the air, the Pt500 sensor and the brick's surface under the same test conditions.

6. Conclusions

In this work a low-order dynamic model was realized to investigate the transient behaviour of an electric oven with the wet clay brick used for the energy consumption test prescribed by the EN 60350

Table 4: Model accuracy in the prediction of the brick heating time and of the total water loss.

T_{set} (°C)	τ_f^{exp} (s)	τ_f^{model} (s)	$\Delta\tau_f$ (%)	$m_{ev\,tot}^{exp}$	$m_{ev\,tot}^{model}$	$\Delta m_{ev\,tot}$ (%)
160	3271	3467	+5.99	198	216	+9.0
180	2867	3014	+5.13	200	218	+9.0
200	2837	2668	-5.96	241	222	-7.9

European standard. The analysis focused on the forced-convective heating function. The heat and mass transfer within the brick were included in the model, taking into account the variation in the brick's thermal capacity due to the water loss and introducing the dependence of the evaporation rate from vapour partial pressures. The dynamics of the Pt500 sensor was also considered.

Given the gray-box nature of the model and the lumped parameter approach used, more than satisfactory agreement between the predicted and the experimental temperatures, brick heating time and water loss was highlighted. Indeed, the percentage deviations between the predicted and experimental temperatures of the air and the brick are comparable to those obtained through CFD models.

The lumped parameter approach ensured a low computational cost, which, together with the good level of accuracy obtained, makes the model suitable as a starting point for model-based control design (e.g. model-predictive control, optimal control). Moreover, because of the capability to capture the difference between the air temperature and the value sensed by the Pt500 probe, the synthesis of advanced control strategies is thus facilitated. In future works, the application of the control theory to obtain a so-called "control-synthesis model" starting from the non-linear model presented here will be introduced. New control laws will be tested on the non-linear model and the possibility of reducing the energy consumption through such control strategies will be investigated.

Among future developments aimed at improving the model reliability, the authors intend to investigate the effects of temperature-dependent evaporation coefficient and partial pressure of water vapour, especially at high temperature. The analysis will also be extended to energy consumption tests carried out in natural convective heating mode.

Acknowledgements

The Authors gratefully acknowledge the support of Electrolux Italia S.p.A. who supplied the oven and funded this research.

Nomenclature

A_i	Area of the surface associated to the generic node i	m^2

c_{dry}	Specific heat capacity of the dry brick	$\mathrm{J \cdot kg^{-1} \cdot K^{-1}}$
c_w	Specific heat capacity of water	$\mathrm{J \cdot kg^{-1} \cdot K^{-1}}$
C_i	Thermal capacity of the generic node i	$\mathrm{J \cdot K^{-1}}$
D	Water evaporation coefficient	$\mathrm{kg \cdot s^{-1} \cdot m^{-2} \cdot Pa^{-1}}$
F_{ij}	View factor between nodes i and j	$-$
G_{ij}	Thermal conductance between nodes i and j	$\mathrm{W \cdot K^{-1}}$
G_{ij}^{rad}	Radiative thermal conductance between nodes i and j	$\mathrm{m^2}$
m_{Br}	Brick total mass	kg
m_{BrS}	Mass associated to the brick's outer part	kg
m_{dry}	Total mass of the dry brick	kg
m_w	Total mass of water absorbed by the brick	kg
$\dot{m}_w$	Water mass flow rate which spreads through the brick and evaporates at the surface	$\mathrm{kg \cdot s^{-1}}$
$m_{w\,ev}$	Cumulative evaporated mass of water	kg
$m_{w\,ev,tot}$	Total evaporated mass of water	kg
n	Number of lumped parameters	
P_{BrS}	Saturation pressure of water at the temperature of brick's outer surface	Pa
P_{BrS}^{exp}	Saturation pressure of water at the experimental temperature of brick's outer surface	Pa
$P_{v\,air}$	Partial pressure of water vapour in the cavity air	Pa
$\dot{Q}_{i\ j}$	Conductive-convective thermal power exchanged between nodes i and j	W
$\dot{Q}_{i\ j}^{rad}$	Radiative thermal power exchanged between nodes i and j	W
r	Brick mass distribution factor	$-$
T_i	Temperature of node i	°C
T_{set}	Oven temperature set-point	°C
$\dot{W}_{el\,i}$	Electric power in input to the i-th heating element	W
Greek letters		
Δ	Absolute deviation between numerical and experimental temperatures	K
Δh_{lv}	Water latent heat of vaporisation	$\mathrm{J \cdot kg^{-1}}$
ΔT_{set}	Oven set-point as increment above ambient temperature	K
ε_i	Emissivity of the surface associated to the generic node i	$-$

σ	Stefan-Boltzman constant	$\mathrm{W} \cdot \mathrm{m}^{-2} \cdot \mathrm{K}^{-4}$
τ	Time	s
τ_f	Total duration of a test, corresponding to the time required to obtain a temperature increment of $55\,K$ at the brick's core	s

Subscripts

AMB	Ambient
BH	Bottom heater
BrC	Brick core
BrS	Brick surface
BW	Bottom wall
D	Glass door
LW	Left wall
OC	Oven centre
Pt	Pt500 temperature sensor
PW	Rear wall
RH	Ring heater
RW	Right wall
TH	Top heater
TW	Top wall

References

[1] E. Hoxha, T. Jusselme, On the necessity of improving the environmental impacts of furniture and appliances in net-zero energy buildings, Science of the Total Environment, 596–597 (2017) pp. 405–416.

[2] D. Amienyo, J. Doyle, D. Gerola, G. Santacatterina, A. Azapagic, Sustainable manufacturing of consumer appliances: Reducing life cycle environmental impacts and costs of domestic ovens, Sustainable Production and Consumption, 6 (2016) 67–76.

[3] P. Bansal, E. Vineyard, O. Abdelaziz, Advances in household appliances - A review, Applied Thermal Engineering, 31 (2011) 3748–3760.

[4] C. E. de Normalisation Electrotechnique (CENELEC), EN 60350-1 Household electric cooking appliances Part 1: Ranges, ovens, steam ovens and grills Methods for measuring performance (latest version including all amendments)., 2013.

[5] J. Cernela, B. Heyd, B. Broyart, Evaluation of heating performances and associated variability of domestic cooking appliances (oven-baking and pan-frying), Applied Thermal Engineering, 62 (2014) 758–765.

[6] J. Abraham, E. Sparrow, A simple model and validating experiments for predicting the heat transfer to a load situated in an electrically heated oven, Journal of Food Engineering, 62 (2004) 409–415.

[7] H. Mistry, S. Ganapathisubbu, S. Dey, P. Bishnoi, J. Castillo, Modeling of transient natural convection heat transfer in electric ovens, Applied Thermal Engineering, 26 (2006) 2448–2456.

[8] H. Mistry, S. Ganapathisubbu, S. Dey, P. Bishnoi, J. Castillo, A methodology to model flow-thermals inside a domestic gas oven, Applied Thermal Engineering, 31 (2011) 103–111.

[9] M. Lucchi, M. Lorenzini, Transient analysis of the radiative heating of rotating PVC pipes in a oven for end-forming process, Applied Thermal Engineering 129 (2018) 84–92.

[10] M. Lucchi, M.Lorenzini, P. Valdiserri, Energy performance of a ventilation system for a block of apartments with a ground source heat pump as generation system, Journal of Physics: Conference Series, 796 (1).

[11] T. McKinley, A. Alleyne, An advanced nonlinear switched heat exchanger model for vapor compression cycles using the moving-boundary method, International Journal of Refrigeration 31 (2008) 1253–1264.

[12] F. Burlon, E. Tiberi, D. Micheli, R. Furlanetto, M. Simonato, Transient model of a Professional Oven, Energy Procedia, 126 (2017) 2–9.

[13] E. Ramirez-Laboreo, C. Sagues, S. Llorente, Dynamic heat and mass transfer model of an electric oven for energy analysis, Applied Thermal Engineering, 93 (2016) 683–691.

[14] E. Ramirez-Laboreo, C. Sagues, S. Llorente, Thermal modeling, analysis and control using an electrical analogy, in: 2014 22nd Mediterranean Conference on Control and Automation, MED 2014, 505–510, 2014.

[15] M. Lucchi, M. Lorenzini, Control-oriented low-order models for the transient analysis of a domestic electric oven in natural convective mode, Applied Thermal Engineering 147 (2019) 438–449.

[16] S. Estrada-Flores, I. Merts, B. De Ketelaere, J. Lammertyn, Development and validation of grey-box models for refrigeration applications: a review of key concepts, International Journal of Refrigeration 29 (2006) 931–946.

[17] M. Lucchi, M. Lorenzini, V. Di Paola, Low-order dynamic model of a domestic electric oven Part I: Experimental characterization of the main heating functions, Journal of Physics: Conference Series 1224 (1).

[18] M. Lorenzini, G. Morini, T. Henning, J. Brandner, Uncertainty assessment in friction factor measurements as a tool to design experimental set-ups, International Journal of Thermal Sciences 48 (2) (2009) 282–289.

[19] N. Lauzier, `https://it.mathworks.com/matlabcentral/fileexchange/5664-view-factors?focused=5060891&tab=function.`, Accessed online on 16th January, 2018.

[20] T. Bergman, A. Lavine, F. Incropera, D. Dewitt, Fundamentals of Heat and Mass Transfer, John Wiley & Sons, Hoboken, 2011.